The role of point defects in PbS, PbSe, and PbTe nanomaterials: a *first principles* study

Wun-Fan Li[1], **Chang-Ming Fang**[1], **Marjolein Dijkstra**[1], **Marijn A. van Huis**[1]

[1] Soft Condensed Matter, Debye Institute for Nanomaterials Science, Utrecht University, Princetonplein 5, 3584CC Utrecht, The Netherlands

E-mail: W.F.Li@uu.nl

Abstract. Intrinsic defects are of central importance to many processes taking place in compound nanomaterials, such as photoluminescence, off-stoichiometry and cation exchange. Here, the role of intrinsic defects in the abovementioined processes inside rock salt (RS) lead chalcogenide systems PbS, PbSe, and PbTe (PbX) were studied systematically using *first principles* density functional theory. Vacancy, interstitial, Schottky, and Frenkel defects were considered. Rock salt PbO was included for comparison. The studied physical properties include defect formation energy, local geometry relaxation, Bader charge analysis, and electronic structure. The defect formation energies indicate that monovacancy defects and Schottky defects are favored over interstitial and Frenkel defects. Schottky dimers, where the cation vacancy and anion vacancy are adjacent to each other, have the lowest defect formation energies at 1.27 eV, 1.29 eV, and 1.21 eV for PbS, PbSe, and PbTe, respectively. Our results indicated that Pb monovacancy gives rise to a shallow acceptor state, while X vacancy generates deep donor state, and Schottky defects create donor-acceptor pairs inside the band gap. The off-stoichiometry of X monovacancies is expected rather than Pb monovacancies due to the lower formation energies of V_X. The surprisingly low formation energy of Schottky dimers suggests that they may play an important role in cation exchange processes, in contrast to the current notion that only single point defects migrate during cation exchange.

PACS numbers: 31.15.es, 71.55.Ht, 73.20.Hb, 81.05.Hd

Density functional theory, Lead chalcogenides, Point defect, Defect state, Photoluminescence, Off-stoichiometry, Cation exchange Submitted to: *J. Phys.: Condens. Matter*

1. Introduction

Lead chalcogenides (PbX, X=S, Se and Te), a family of narrow band gap IV-VI semiconductors, have been the subject of intensive research due to their applications in many fields such as thermoelectric energy converters[1, 2], thermal photovoltaic devices[3], infrared lasers[4], and light-emiting diodes.[5] Together with the CdX chalcogenides family (CdS, CdSe, CdTe), the PbX systems are abundantly used in heterogeneous nanocrystals (HNCs) to create new materials with novel and tunable physical properties.[6, 7, 8]

By physical nature, defects inevitably exist in crystals, and play a pivoting role in the growth, synthesis and in many physical properties of HNCs and multicomponent quantum dots (QDs). First, point defects, depending on the position of their defect states with respect to the band gap, can determine whether the process of the electron-hole recombination in nanocrystals is radiative or non-radiative[9, 10]. Thus point defects directly affect the quantum yield of nanocrystal (NC) QDs. Second, there is much unclarity in the literature about how the off-stoichiometry of the NCs[11, 12], a typical product of wet chemical synthesis, affects the physical properties. In particular, it is at present unclear whether the excess or depletion of anions or cations is accomodated only at the surface, or also at the interior of the NCs. Third, the very important cation exchange (CE) process that is used to create core-shell type structures and synthesis of NCs in deviating crystal structures[13, 14, 15, 16, 17, 7, 18, 19, 20], requires the migration of cations, as shown in many experimental studies. In RS chalcogenides, this is assumed to be mediated by cation vacancies[20, 7]. Groeneveld *et al.* proposed that ZnSe-CdSe colloidal quantum dots (QD) can be tailored via a CE mechanism mediated by Frenkel pairs of Zn interstitials Zn_i and Zn vacancies V_{Zn}.[18] Marianna *et al.* brought forth a plausible mechanism that the growth of PbSe/CdSe core/shell nanocrystal is formed by CE, where the cation vacancies assist the migration of cations.[7] Yingzhuo *et al.* proposed that CdSe/ZnSe core/shell QD can be synthesized in aqueous environment through CE.[19] Finally, Yalcin *et al.* recently found that the CE in the solid-solid-vapor (SSV) growth of PbSe/CdSe core/shell HNCs is mediated by Cd vacancies at the PbSe-CdSe interface.[20] However, it is difficult, or even impossible to determine experimentally which types of defects are present in the material and what their role is in, e.g., CE progresses. It is only until recently, that more insight of CE was unveiled by *first principles* calculations of Ag ions in wurtzite CdSe[21]. To the best of our knowledge, our current work is the first DFT study discussing point defects in RS PbX in the context of the CE precess. Although in all the experimental literature given avobe, monovacancies are presumed to enable CE, we give an important finding that vacancy comlexes, $i.e.$, Schottky defects, can not be excluded in CE because they possess significantly lower formation energies than monovacancies do. In all these phenomena, the presence of vacancies and other point defects is a crucial parameter. In this work, we identify and characterize the most important point defects in PbX chalcogenides, and discuss their role in the abovementioned processes.

In the current study, four kinds of point defects are considered. These are vacancy, interstitial, Schottky dimer/pair, and Frenkel pairs. These defects are schematically shown in Fig. 1. Vacancies and interstitials contain only one defect site, while Schottky and Frenkel defects include two defect sites. A Schottky defect consists of a cation-anion vacancy pair. Schottky dimer is defined as the cation vacancy and the anion vacancy sites being adjacent to each

other, and in the Schottky pair configuration, the two defect sites are separated as far as possible within a supercell. A Frenkel defect is created when an atom moves from its original place to an interstitial site, whereby a vacancy site and an interstitial site are generated. In binary compounds such as PbX, both the cation Frenkel defect and the anion Frenkel defect need to be considered.

Defects in PbX have received much attention by scientists for decades. The related research has been carried out both experimentally[22, 23, 24, 25, 26, 27] and theoretically. [28, 29, 30, 23, 31, 32, 33, 34, 35, 36, 37, 38] Miller *et al.* found that the formation energy of a Frenkel defect is higher than a Schottky defect in PbTe, hence the diffusion is essentially controlled by a vacancy-type mechanism.[22] By using positron annihilation technique, Polity *et al.* established the relationship between V_{Pb} concentration and positron lifetime.[23] Yoneda *et al.* reported that Schottky defects will form in PbTe when the crystal is heated over 200 °C.[25] Via the measurements of step-scan Fourier-transform infrared photoreflectance (step-scan FTIR PR) on a PbTe thin film, the defect state of V_{Te} was found at 29.1 meV above the conduction band maximum (CBM), and another defect state at 18.1 meV below the valence band maximum (VBM) may be attributed to V_{Pb} or threading dislocations, whereas no states were found in the band gap.[26] Koumoulis performed NMR measurements on PbSe, and reported p-type shallow acceptor state and n-type deep state at midgap.[27]

Theoretical calculations were also performed on PbX systems. Berashevic carried out a detailed study on vacancy defects in α-PbO (litharge structure)[36], and found the charged defect states for V_{Pb}^{2-} at 0.1 eV below the VBM, and V_O^+ at 1.03 eV above the VBM, which were stabilized by charge transfer. For PbS, Ding *et al.* studied the $(\bar{1}00)$ surface, and found the p-type V_{Pb} and n-type V_S defect states. They also found that the structural relaxation at the surface is opposite to the case of bulk PbS: around the defect site, the nearest-neighboring (NN) atoms of the defect site will be repelled outwards, while the next-nearest-neighboring (NNN) atoms will move toward the defect site.[32] Walsh studied vacancy defects and Schottky defects in their neutral and charged states.[34] The Schottky defect was found to be preferred over vacancy defects as it has a lower formation energy. Donghun *et al.* found for PbS quantum dots (QD) that off stoichiometry will introduce new states which are highly localized on certain surface atoms.[38] For PbSe, Peng *et al.* performed a series of calculations for bulk PbSe doped with 26 substitutional impurities.[35] Wrasse *et al.* studied the electronic structure of both bulk and nanowire PbSe with group III substitutional impurities.[37] For PbTe, there are a series of theoretical studies concerning the defect states: Parada and Pratt made the first attempt to describe the electronic structure of defective PbTe using the Slater-Koster model, [28, 29] and Lent *et al.* used a tight-binding method to give a qualitative description of the deep defect state in PbTe.[30] However the calculations in Refs. [28, 29, 30] are non-self-consistent calculations. Recently, Ahmad and Hoang employed self-consistent DFT calculations for vacancies and substitutional impurities in both bulk[31, 33] and thin-film[33] PbTe. Furthermore, there are several other theoretical investigation done on perfect PbX systems for structural and electronic properties[39, 40, 41, 42], and thermodynamic properties.[43, 44, 45] All of these studies are limited to perfect PbX crystals, though, thus no defect was induced.

The formation energy of defects is key to verify which kind of defect(s) are more likely to be formed inside a crystal, and thus may determine the CE process. Using the *first principles* DFT approach, we firstly aim to

compare the relative stability of the defect species inside PbX in terms of defect formation energy, so that we can identify which defects may be involved in the CE process. Second, we would like to provide a fundamental and panoramic view of the physical properties of the point defects inside PbX, which is indispensible for further study and applications of these materials. Besides defect formation energies, the physical properties including local geometry relaxation, charge transfer, and electronic structure, were analyzed. The typical point defects for these compounds are: vacancy, interstitial, Schottky, and Frenkel. Even though PbO occurs in the litharge structure rather than the rock salt (RS) phase[46], we include the calculations of RS PbO for comparison.

The content of this paper is organized as follows: the computational details are given in Sec. II. The results and discussions are presented in Sec. III and IV, respectively; first we will compare the relative stability of all the defect types, after which we select the more stable ones for a more detailed study of physical properties. Finally, conclusions are given in Sec. V.

2. Computational Details

2.1. Computational Settings

All the calculations were carried out using the *first principles* DFT code VASP[47, 48, 49] within the Projector-Augmented Wave (PAW) framework.[50] The Generalized Gradient Approximation (GGA) formulated by Perdew, Burke, and Ernzerhof (PBE) [51] was employed for the exchange and correlation energy terms. The cut-off energy of the wave functions was 500 eV. The cut-off energy of the augmentation functions was 700 eV. Due to computational limitations, we used only the embedded scalar relativistic effect in the VASP code, and the spin-orbit coupling (SOC) is not explicitly included in our calculations. For supercells, the sampling in the reciprocal space was done by using a $2 \times 2 \times 2$ *k* mesh with 4 or 6 irreducible *k* points depending on the symmetry of the systems. For the unit cell of PbX and elemental Pb, a $24 \times 24 \times 24$ *k* mesh containing 455 irreducible *k* points was used. And for elemental S, due to the large unit cell size, a $4 \times 4 \times 2$ *k* mesh was used with 18 irreducible *k* points. For elemental Se and Te, a $24 \times 24 \times 20$ mesh with 1103 irreducible *k* points was used. All the *k* meshes were Γ-centered in the reciprocal space.

In our study, we used $3a_0 \times 3a_0 \times 3a_0$ RS supercells containing 216 atoms for all the four PbX systems. Here a_0 is the lattice constant, and the optimized a_0 is 5.233 Å for PbO, 5.994 Å for PbS, 6.207 Å for PbSe, and 6.561 Å for PbTe. Also the band gaps of the relaxed PbX systems are calculated. These calculated values are compared with selected literature values in Table 1 for lattice constants and in Table 2 for band gaps. The calculated lattice parameters of PbX are slightly larger than the corresponding experimental values (1.0% ~1.5%). This is not unusual for the DFT-GGA approach[51]. Note that the band gap of PbTe is larger than the experimental value of 0.31 eV, in contrast with the notion that DFT normally underestimates the band gap. Such a large band gap of PbTe comes from the inherited property of the PAW basis set[42]. The LAPW approach by Wei and Zunger[39] and the Quasi-particle GW calculatin by Svane *et al.*[52] provide more accurate values for the band gaps, however these methods are computationally expensive and not feasible for the current defect studies, which require large simulation cells. The supercells were built using the optimized lattice constant from the corresponding unit cells. The structural models are shown in Fig. 1. The defect sites were put as far as possible from each other to avoid

artificial interactions among them. In order to determine the defect formation energy, we need to calculate the energy of the constituent elements in each compound was calculated to serve as reference energies. Elemental Pb was calculated using a 4-atom Face-Centered Cubic (FCC) unit cell. For elemental anion phases, we employed molecular triplet O_2 for oxygen, 128-atom unit cell for α-sulfur, and a 3-atom trigonal unit cell for selenium and tellurium, respectively. The calculated energies are -3.572 eV/atom (Pb), -4.959 eV/atom (O), -4.126 eV/atom (S), -3.483 eV/atom (Se), and -3.142 eV/atom (Te).

Both the supercell shape and atomic positions were allowed to relax during geometry optimization. The optimization was considered as converged if the difference in energy between two subsequent electronic optimization steps was smaller than 1.9×10^{-4} eV, while the forces on the atoms were smaller than -0.02 eV/Å.

2.2. Defect formation energies

In order to allow a comparison of the relative stability of these defects inside a crystal, we need to first define the formulas to calculate defect formation energies. This choice of definitions allows direct comparison with phase diagrams.[59, 60, 61, 62] In the pseudo-binary phase diagrams, the stoichiometric configuration of these three compounds (with 50% atomic percent of the anions) are all very stable at high temperatures as the melting point of the three compounds at stoichiometric configuration is 1118 °C for PbS, 1079 °C for PbSe, and 924 °C for PbTe, respectively. Thciteore the choice of stoichiometric perfect PbX, and elemental phases of Pb cation and the X anions as reference states for calculating the defect formation energy is reasonable. Here the number of atoms is always conserved, and all defects are neutral.

The general fomula of defect formation

Table 1. Calculated lattice constants a (Å) of the relaxed unit cell for PbX systems compared with previous theoretical and experimental[53] results. The methods of calculation are given by *basis set-xc functional*.

PbX	LAPW-PZ81[a]	PAW-PBE[b]	PAW-HSE03[b]	PAW-PBE[c]	PAW-PBEsol[d]	PAW-PBE[e]	This work (PAW-PBE)	Exp.[f] at 300 K
PbO	–	–	–	–	–	5.27	5.233	–
PbS	5.906	6.004	5.963	5.992	5.905	–	5.994	5.936
PbSe	6.098	6.214	6.170	6.200	6.104	–	6.207	6.124
PbTe	6.439	6.568	6.519	6.556	6.448	–	6.561	6.462

[a] Ref. [39]. LAPW: Linearized Augmented Plane Wave. PZ81: The Perdew-Zunger functional[54]
[b] Ref. [42]. HSE03: The hybrid functional developed by J. Heyd, G. E. Scuseria, and M. Ernzerhof.[55]
[c] Ref. [43]
[d] Ref. [56]. PBEsol: A new PBE intended for solid state and surface systems. [57]
[e] Ref. [46]
[f] Ref. [53]

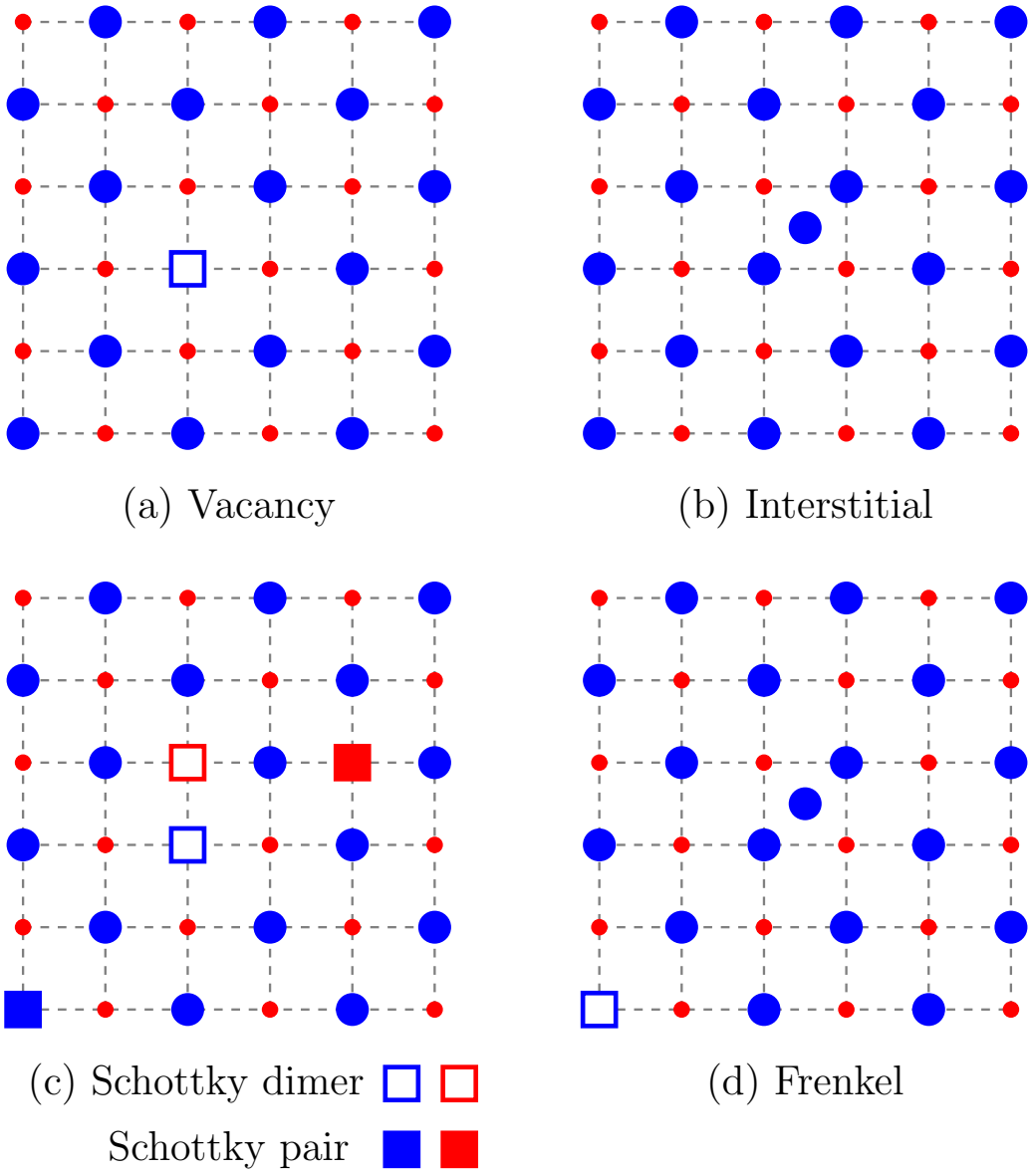

Figure 1. 2D Schematic of the supercell models used in this study. The models are $3 \times 3 \times 3$ PbX supercells with the RS structure. Pb atoms are depicted in red, and X atoms in blue. Vacancy and interstitial defects can be either at the Pb or X site. The interstitial atom is at the tetrahedral site formed by its counter atoms. (the interstitial Pb atom is surrounded by four Pb atoms and four X atoms, and vice versa.) Schottky dimer and Schottky pair are shown in the same supercell only for showing their configurations, in calculations they are introduced in two separate supercells. The Frenkel defect can be both for Pb atoms or for X atoms. Note that the inter-defect distance in the Schottky and Frenkel configuration is longer than that were used in 3D models.

Table 2. Calculated band gaps E_g (eV) of the relaxed unit cell for PbX systems compared with previous theoretical and experimental[53] results. The methods of calculation are given by *basis set-xc functional*.

PbX	LAPW-PZ81[a]	PAW-PBE[b]	PAW-HSE03[b]	PAW-PBE[c]	PAW-GW[d]	PAW-PBEsol[e]	This work (PAW-PBE)	Exp.[f] at 300 K
PbO	–	–	–	–	–	–	0.99	–
PbS	0.29	0.37	0.67	0.44	0.20	0.31	0.47	0.37-0.40
PbSe	0.17	0.30	0.58	0.31	0.18	0.21	0.43	0.26-0.29
PbTe	0.19	0.73	0.98	0.81	0.65	0.29	0.83	0.29-0.32

[a] Ref. [39]. LAPW: Linearized Augmented Plane Wave. PZ81: The Perdew-Zunger functional.[54]
[b] Ref. [42]. HSE03: The hybrid functional developed by J. Heyd, G. E. Scuseria, and M. Ernzerhof.[55]
[c] Ref. [43]
[d] Ref. [52]
[e] Ref. [56]. PBEsol: A new PBE intended for solid state and surface systems.[57]
[f] Ref. [58]

energy is[63, 64],

$$E^f = E_{defect} - E_{perfect} - \sum_i \Delta n_i(\mu_i) + q\epsilon_F, \quad (1)$$

whereby E^f is the formation energy, E_{defect} the total energy of the defect cell, $E_{perfect}$ the total energy of the perfect cell. The Δn_i's are the number of atoms added ($\Delta n_i > 0$) to or subtracted ($\Delta n_i < 0$) from the perfect cell and the μ_i's are the atomic chemical potentials for these atoms. q is the charge of the defect and ϵ_F is the Fermi energy, i.e. the electronic chemical potential.

This expression simplies for the calculations described in this paper; the possibility of charged defects has not been considered and thciteore $q = 0$ in Eq. 1, so that the last term vanishes. The atomic chemical potentials μ can be regarded as the atomic reservoir with which the atoms are exchanged. For off-stoichiometric defects (vacancies and interstitials in our case), we set $\mu_{Pb} = E(Pb)$ and $\mu_X = E(X)$, where $E(Pb)$ and $E(X)$ are the energies of Pb metal and elemental phases of chalcogen atoms X, respectively. If we define $N = 108$ as the number of one atomic specie inside the PbX supercell, then $E_{perfect}$ becomes $E(Pb_N X_N)$, and the following equations can be obtained for vacancies and interstitals:

Vacancies:

$$E^f_{v,Pb} = E(Pb_{N-1}X_N) - E(Pb_N X_N) + E(Pb), \quad (2a)$$

$$E^f_{v,X} = E(Pb_N X_{N-1}) - E(Pb_N X_N) + E(X). \quad (2b)$$

Interstitials:

$$E^f_{i,Pb} = E(Pb_{N+1}X_N) - E(Pb_N X_N) - E(Pb), \quad (2c)$$

$$E^f_{i,X} = E(Pb_N X_{N+1}) - E(Pb_N X_N) - E(X). \quad (2d)$$

For stoichiometric defects, i.e. Schottky and Frenkel, the bulk PbX is regarded as the reference

atomic reservoir, thciteore $\mu_{Pb} + \mu_X = E(PbX)$, where $E(PbX)$ is the energy of bulk PbX per PbX Pair. The defect formation energies are then evaluated by the following equations:

Schottky defects:

$$E^f_{Schottky} = E(Pb_{N-1}X_{N-1}) - \frac{107}{108}E(Pb_NX_N). \tag{3a}$$

Frenkel defects:

$$E^f_{Frenkel} = E(Pb_NX_N)_{Frenkel} - E(Pb_NX_N). \tag{3b}$$

2.3. Charge density difference

The charge density difference can be used to describe the charge density changes caused by a defect inside a system. It is defined for the chosen defects as follows[65]:

$$\Delta\rho = \rho(defect) - [\rho(Pb\ sublattice) + \rho(X\ sublattice)], \tag{4}$$

which is the difference of charge density between the defective system and the sum of its cation and anion sublattices. We compare $\Delta\rho$ of the nearest-neighboring (NN) atoms around the defect site with $\Delta\rho$ of other atoms more distant from the defect site, then the influence on charge distribution from defect sites can be clearly seen. We also examined the influence of geometry relaxation on charge density difference by comparing the $\Delta\rho$ patterns calculated using the initial geometries and the relaxed final geometries. We found that the two $\Delta\rho$ patterns are almost identical, indicating that geometry relaxation has very little effect on charge density difference. In this work, the charge density difference was calculated using the relaxed structures.

3. Results

We separate the discussion of point defects (single defect site: vacancy and interstitial) and stoichiometric defects (double defect sites: Schottky and Frenkel) as these two groups have different defect configurations. We first compare the formation energy of these defects to determine their relative stability, and choose the more stable ones for further discussion of local relaxation, charge distribution and electronic structure.

3.1. Defect formatiom energy

The results of defect formation energies are shown in Fig. 2 and Table 3. For RS PbO, only the cation and anion vacancies are structurally stable. Interstitials, Schottky and Frenkel defects in RS PbO all led to litharge-like structures during the geometry relaxation. Thciteore we only include vacancy formation energies for RS PbO here.

The defect formation energy exhibits certain trends along O $\rightarrow$ S $\rightarrow$ Se $\rightarrow$ Te. Along the direction of increasing atomic size of the chalcogen atom, the formation energy of V_{Pb}, V_X and anion Frenkel are increasing, but the formation energy of cation Frenkel defects, Schottky dimer and Schottky pair are decreasing. Only the formation energy of interstitials shows a dip for PbSe.

Comparing the magnitude of formation energy of these defects, it is clear that vacancies and Schottky defects are lower than those of interstitial and Frenkel defects (except that I_{Pb} is lower than V_X for PbSe) , as shown in Fig. 2 and Table 3 Although $E^f_{v,Pb}$ and $E^f_{v,X}$ can not be compared directly since they were calculated with different stoichiometries and different formulas, the current results indicate that vacancy-type defects are dominant, and thciteore CE may be driven by the more easily formed

cation vacancies.[20, 66] Schottky defects are also energetically favored defects, but they were not seriously considered for the CE processes. Frenkel defects in PbX systems have a much higher formation energy than Schottky defects because the interstitial sites within the Frenkel configuration induce a considerable distortion due to local expansion of the lattice. For Schottky defects, the Schottky dimer is always more favored than the Schottky pair.

There are only a handful of defect formation calculations done by $ab-initio$ DFT methods for PbX.[34, 33, 67] The results from literature and our calculations are collected in Table 3. Our calculated values of formation energies of neutral defects in PbS are higher than those from Walsh[34] by 0.67 eV and 0.72 eV for V_{Pb}, V_S, respectively. The formation energy of the Schottky defect can not be compared since we do not know whether a Schottky dimer or a Schottky pair was studied in Ref. [34]. The systematic discrepancy in defect formation energies may originate from the fact that the supercells were not fully relaxed, and due to the larger supercell size (512 atoms), and less k-point (Γ only) used in Ref. [34]. Hoang *et al.*[33] calculated E^f of V_{Pb} and V_{Te} for PbTe using DFT-GGA, $2a_0\times2a_0\times2a_0$ supercells, and cut-off energy of 300 eV. Their reported values are 2.187 eV and 2.135 eV for V_{Pb} and V_{Te}, separately. These values are very close to our results of 1.896 eV (ΔE =0.291 eV) for V_{Pb} and 2.129 eV (ΔE =0.006 eV) for V_X. Chai *et al.* reported the Schottky dimer formation energy of PbSe to be 1.47 eV. They used a smaller supercell of $2a_0 \times 2a_0 \times 2a_0$, and 450 eV of cut-off energy. The difference between 1.47 eV and our value of 1.29 eV is thus expected and is due to the different computational settings.

The defect formation energy is caused by a sum of effects, being mainly, 1) ionic size, 2) Coulomb interactions, 3) swelling or shrinkage of the lattice, and 4) the local relaxations around the defect site, which may all play a role in determining the magnitude of the formation energy of defects. These effects will be addressed in the following sections.

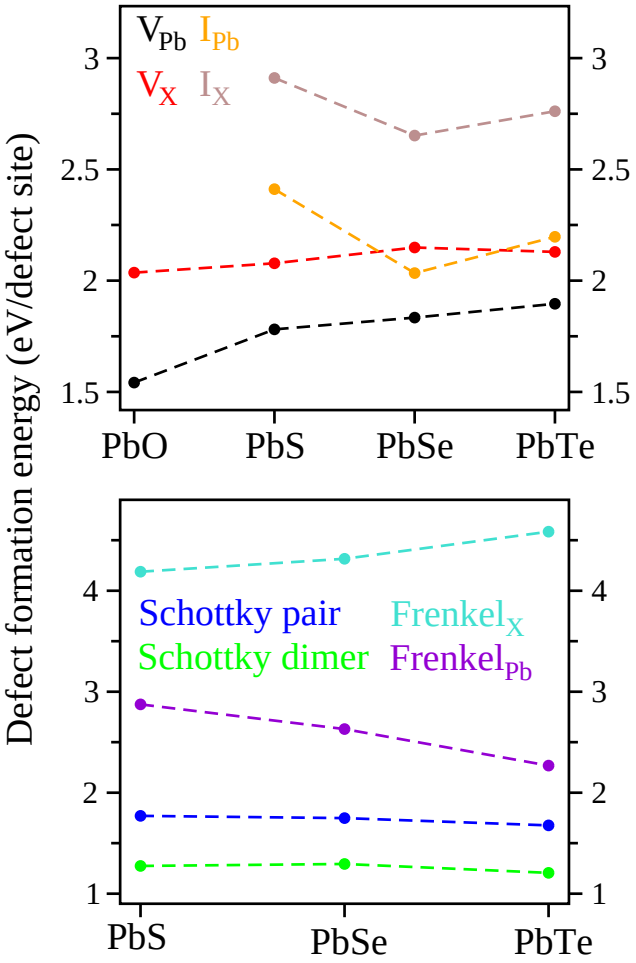

Figure 2. Formation energy of defects in PbX. Different defect types are labeled with different colors. Dotted lines are drawn to guide the eye.

3.2. Local geometry relaxation

The comparison of the local relaxation around the defect site is listed in Tables 4 , 5 and 6. In order to describe the pictures more clearly, we call the NN Pb atoms of a X vacancy as $Pb^{NN(V_X)}$, and the NN X atoms of a Pb vacancy site as $X^{NN(V_{Pb})}$. For V_{Pb}, the $X^{NN(V_{Pb})}$ expand outward, but the extent of the expansion becomes smaller with increasing atomic size of the X atoms. For V_X, there is not

Table 3. Defect formation energy (eV/defect) of the intrinstic defects selected in this study.

PbX	V_{Pb}		V_X		I_{Pb}		I_X	
	This work	Lit.	This work	Lit.	This work	Lit.	This work	Lit.
PbO	1.54	-	2.04	-	-	-	-	-
PbS	1.78	1.36[a]	2.08	1.77[a]	2.41	-	2.91	-
PbSe	1.83	-	2.15	-	2.03	-	2.65	-
PbTe	1.90	2.19[b]	2.13	2.14[b]	2.20	-	2.76	-

PbX	Schottky dimer		Schottky pair		Frenkel Pb		Frenkel X	
	This work	Lit.	This work	Lit.	This work	Lit.	This work	Lit.
PbS	1.27	1.04[b]	1.77	-	2.87	-	4.19	-
PbSe	1.29	1.47[c]	1.75	-	2.63	-	4.32	-
PbTe	1.21	-	1.68	-	2.27	-	4.58	-

[a] Ref. [34]. GGA-PBE, cut-off energy = 500 eV, $4a_0 \times 4a_0 \times 4a_0$ supercell, Γ-point-only k-mesh, geometry relaxation not specified.

[b] Ref. [33]. GGA-PBE, cut-off energy = 300 eV, $2a_0 \times 2a_0 \times 2a_0$ supercell, k-mesh not specified, geometry fully relaxed. Did not specify either it is a Schottky dimer or a Schottky pair.

[c] Ref. [67]. GGA-PBE, cut-off energy = 450 eV, $2a_0 \times 2a_0 \times 2a_0$ supercell , $8 \times 8 \times 8$ k-mesh, geometry fully relaxed.

a simple trend found; the $Pb^{NN(V_X)}$ may shrink inward or expand outward. In the study of V_{Pb} and V_{Te} in PbTe[33], it was found that the NN Te atoms around V_{Pb} expand by ~0.024 Å, and the NN Pb atoms of V_{Te} relax inward by 0.07 Å.

The interstitial defects result in a large structural distortion to the crystal, which may be the reason for the higher defect formation energy for interstitials.

For Schottky defects, both for the Schottky dimer and Schottky pair, the NN atoms of the cation and anion vacancy sites expand outward during relaxation. $Pb^{NN(V_X)}$ relax more outwards than $X^{NN(V_{Pb})}$. Along the direction of S→Se→Te, the degree of expansion is decreasing for the NNs of V_{Pb}, but increasing for the NNs of V_X. The reason for these trends is that the atomic size is growing along S→Se→Te (Table 8). With the larger atomic size, it is more difficult to displace the anion atoms, which results in the decreasing magnitude of expansion for $X^{NN(V_{Pb})}$. On the other hand, the expansion of the $Pb^{NN(V_X)}$ is a net result of the electrostatic interactions, which will be addressed in subsection 3.4. The $X^{NN(V_{Pb})}$ (except for PbS) and $Pb^{NN(V_X)}$ expand slightly more in Schottky pair than in Schottky dimer, which implies that the binding interaction within Schottky dimer attracts the NN atoms more. Here we discussed qualitatively how the relaxations affect atomic mobility. For a quantitative assessment, energy barriers would need to be calculated, which is beyond the scope of this work.

In Frenkel defects, all of the nearest neighbors of the defect sites underwent expansion. Especially at the interstitial sites, the huge expansion of their NN atoms could be the reason why the Frenkel defects are less stable.

3.3. Bader charge

The Bader charge for the NNs of each defect site is presented in Table 7 and in Fig. 3. We also listed the ionic radius and electronegativity of the anions in Table 8. As the atomic number

Table 4. Relative displacement of the nearest neighbors of vacancy and interstitial sites. d_i denotes the initial distance, where d_{Pb-X} is the distance between Pb and the nearest X atom, and $d_{Pb-X,int}$ is the distance between an interstitial atom and its nearest neighbor. d_f is the final Pb-X distance in relaxed supercells. Δr is the distance displacement defined as $\Delta r = d_f - d_i$, and $\Delta r(\%)$ is Δr scaled with respect to d_i. The unit of length is Å.

	d_i		V_{Pb}			V_X			I_{Pb}			I_X		
	$d_{\text{Pb-X}}$	$d_{\text{Pb-X, int}}$	d_f	Δr	$\Delta r(\%)$	d_f	Δr	$\Delta r(\%)$	d_f	Δr	$\Delta r(\%)$	d_f	Δr	$\Delta r(\%)$
PbO	2.618	–	2.787	0.169	6.46	2.680	0.062	2.37	–	–	–	–	–	–
PbS	2.997	2.595	3.078	0.081	2.70	2.963	-0.034	-1.13	2.855	0.260	10.02	2.759	0.164	6.32
PbSe	3.103	2.668	3.156	0.053	1.71	3.155	0.052	1.68	2.948	0.280	10.49	2.946	0.278	10.42
PbTe	3.280	2.841	3.285	0.005	0.15	3.150	-0.130	-3.96	3.130	0.289	10.17	3.134	0.293	10.31

Table 5. Relative displacement of the nearest neighbors of Schottky defect sites

	d_i	Schottky dimer						Schottky pair					
	$d_{\text{Pb-X}}$	V_{Pb}			V_X			V_{Pb}			V_X		
		d_f	Δr	$\Delta r(\%)$	d_f	Δr	$\Delta r(\%)$	d_f	Δr	$\Delta r(\%)$	d_f	Δr	$\Delta r(\%)$
PbS	2.997	3.091	0.094	3.14	3.142	0.145	4.84	3.072	0.075	2.52	3.158	0.161	5.37
PbSe	3.103	3.153	0.050	1.61	3.273	0.170	5.48	3.156	0.053	1.71	3.313	0.210	6.77
PbTe	3.280	3.283	0.003	0.09	3.483	0.203	6.19	3.300	0.020	0.61	3.508	0.228	6.95

Table 6. Relative displacement of the nearest neighbors of Frenkel defect sites

	d_i		Frenkel$_{Pb}$						Frenkel$_X$					
			V_{Pb}			I_{Pb}			V_X			I_X		
	d_{Pb-X}	$d_{Pb-X,\,int}$	d_f	Δr	$\Delta r(\%)$	d_f	Δr	$\Delta r(\%)$	d_f	Δr	$\Delta r(\%)$	d_f	Δr	$\Delta r(\%)$
PbS	2.997	2.595	3.089	0.092	3.07	2.848	0.253	9.72	3.185	0.188	6.27	2.703	0.107	4.16
PbSe	3.103	2.668	3.163	0.060	1.93	2.941	0.273	10.23	3.308	0.205	6.61	2.852	0.184	6.90
PbTe	3.280	2.841	3.306	0.026	0.79	3.107	0.266	9.36	3.491	0.211	6.43	3.071	0.230	8.10

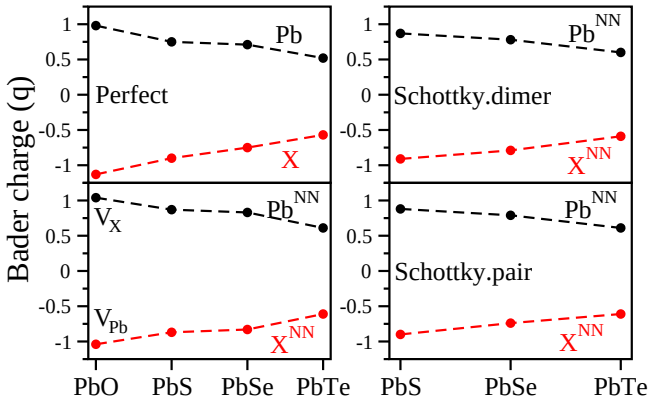

Figure 3. Bader charge of the defect sites. The black dots denote the results for the Pb atoms, and the red dots for the X atoms.

increases, the ionic radius of the chalcogen ions increases, and their electronegativity decreases. Thus, one can expect that the extent of the ionic characteristics in the Pb-X bonding will also decrease with O → S → Se → Te, resulting in less charge transfer. This is clearly seen in Fig. 3. For both defect-free and defective PbX systems, the Bader charge of both Pb and X atoms decreases with O → S → Se → Te. It is noteworthy that the charge on either the cation or the anion is not greater than 1 *e*, which matches the previously calculated value of 0.85 *e* for Pb and -0.85 *e* for S in bulk PbS.[68] This suggests that the classical ionic model of $Pb^{2+}X^{2-}$ can be applied to PbX only for qualitative approximation, and the bonding within these systems is covalent in nature.[69]

3.4. Charge density difference

The results for the charge density difference are shown in Fig. 4 as 2D intensity plots and in Fig. 5 as line profiles. We show only the V_{Pb}, V_X, and Schottky dimer defects in Fig. 4. The results of Schottky pair is included in the Supporting Information (SI). In Fig. 4 (a)–(d), we also show $\Delta\rho$ for perfect PbX crystals obtained by Eq. 4.

Table 7. Bader charge of the nearest neighboring (NN) atoms of vacancy, Schottky dimer and Schottky pair defects.

	perfect		V_{Pb}	V_X	Schottky dimer		Schottky pair	
	Pb	X	X^{NN}	Pb^{NN}	Pb^{NN}	X^{NN}	Pb^{NN}	X^{NN}
PbO	1.04	-1.04	-1.13	0.99	–	–	–	–
PbS	0.87	-0.87	-0.90	0.75	0.88	-0.91	0.88	-0.90
PbSe	0.83	-0.83	-0.73	0.71	0.78	-0.79	0.79	-0.74
PbTe	0.61	-0.61	-0.56	0.52	0.60	-0.59	0.58	-0.58

Table 8. Ionic radius r_{ion}, electronegativity χ and Bader charge (in perfect PbX supercell) of O, S, Se, and Te.

X	r_{ion} of X^{-2} (Å)[a]	χ (Pauling scale)	Bader charge (q)
O	1.26	3.44	-1.04
S	1.70	2.58	-0.87
Se	1.84	2.55	-0.83
Te	2.07	2.10	-0.61

[a] Ref. [70]

This is included for comparison with defective crystals.

3.4.1. V_{Pb} defects Fig. 4 (e)–(h) show $\Delta\rho$ for V_{Pb} in PbX. After comparing with the perfect lattices, only the NN anions of the vacancy site have a clear change in $\Delta\rho$. This means that the perturbation of charge density introduced by the Pb vacancy inside the crystal is very localized. PbO behaves quite differently to the other PbX systems. The charge density is evenly distributed around the nucleus in an almost unperturbed way. This accumulation of charge density may be caused by the fact that the oxygen p orbitals are more tightly bound to the nuclei, so that the electron density is trapped at these orbitals.PbS, PbSe, and PbTe all exhibit similar $\Delta\rho$ patterns. In these three systems, the polarization of the electron density indicates that the NN anions possess two kinds of interactions: First, the NN anions mutually repel each other due to Coulomb interaction caused by the absence of the Pb atom at the vacant site. And second is the interaction with their neighboring Pb cations: between the NN anions and their Pb neighbors, there is an accumulated charge density, and this charge density is polarized toward the Pb cations. The net results of these two interactions are the polarized charge density of the NN anions and the expanded relaxation of the Pb-X distance around V_{Pb}, as shown in Table 4. The extent of this polarization decreases with O $\rightarrow$ S $\rightarrow$ Se $\rightarrow$ Te, reflecting the fact that the ionicity of the chalcogen anions decreases along O $\rightarrow$ S $\rightarrow$ Se $\rightarrow$ Te.

3.4.2. V_X defects The electron density is polarized in the case of V_X as well (Fig. 4 (i) –(l)). In the case of V_X, the NN Pb atoms relax toward the vacancy site (although the NN Pb atoms of V_X in PbO and PbSe shifted outwards from the vacancy site), accompanied by an asymmetric polarization of the NN Pb charge density toward the vacancy site. Even the NNN anion atoms donate some charge density to the vacancy center. This polarization results in a slight accumulation of charge density at the anion vacancy site, and resembles the notion of *electrides*. Electrides are

crystals where electrons occupy anion vacant sites and act as anions.[71, 72, 73, 74] In order to capture the accumulated electron density at the anion vacancy site, we also plotted the line profile for each V_X defect of PbX, as shown in Fig. 5. One can clearly see that, except for PbO, all the PbX have excess charge density at the anion vacancy site.

We also evaluated the amount of charge inside a sphere at the vacancy site. The chosen radii and integrated charges are shown in Table 9. The radii of the spheres are defined by checking the charge density of Pb and X ions in perfect PbX systems: the charge density minimum between Pb and X ions are set as boundary of the two ionic radii. The integrated charges are 0.53 e for PbS, 0.37 e for PbSe, and 0.57 e for PbTe. These values prove qualitatively that charges are attracted toward the anion vacancy site upon the presence of the anion vacancy, generating an electride inside the lattice.

Table 9. Charges integrated inside a sphere located at the anion vacnacy defect site in PbX systems.

PbX	$r_{Pb}(\AA)$	$r_X(\AA)$	Charge (e)
PbS	1.39	1.60	0.53
PbSe	1.46	1.66	0.37
PbTe	1.48	1.79	0.57

3.4.3. Schottky dimer The charge density difference of Schottky dimer is shown in Fig. 4 (m)–(o). The pattern of $\Delta\rho$ for V_{Pb} and V_X in the Schottky dimer is very similar to the case where they exist individually ($cf.$ (e)–(l) of Fig. 4), however in this case the Pb atom is absent at the V_{Pb} site, thciteore the charge density of its NN X atoms is more polarized towards the V_X site.

The charge density difference plots can also explain why the NN Pb atoms of the V_X site expand more along S $\rightarrow$ Se $\rightarrow$ Te in Schottky configurations, which is described in subsection 3.2. As shown in Fig. 4, the charge density of $Pb^{NN(V_X)}$ are polarized toward the V_X site as they do in the V_X case, but the extent of polarization decreases drastically along S $\rightarrow$ Se $\rightarrow$ Te. On the other hand, these $Pb^{NN(V_X)}$ also undergo an attraction from the neighboring X atoms through the polarized charge density between the two sides, and this attraction remains significant along S $\rightarrow$ Se $\rightarrow$ Te. Thciteore, the net result is that the $Pb^{NN(V_X)}$ will be attracted more toward their neighboring X atoms along S $\rightarrow$ Se $\rightarrow$ Te.

3.5. Electronic structure

Band structure and density of states (DOS) calculations have been done for V_{Pb}, V_X, Schottky dimer and Schottky pair defect configurations, and the details are included in the SI. Since the smallest band gap occurs at the L point in the first Brillouin zone, we summerized all the positions of the defect states at the L point into Fig. 6. As one can see, along the direction of O $\rightarrow$ S $\rightarrow$ Se $\rightarrow$ Te, the V_X position shifts toward CBM, forming a deep defect state lying in the band gap. On the other hand, the V_{Pb} state generates a shallow state near the VBM margin, and the position of this state does not vary along O $\rightarrow$ S $\rightarrow$ Se $\rightarrow$ Te. For Schottky dimer (SD) and Schottky pair (SP) defects, we see that both the V_{Pb} and V_X states appear at the position similar to their single vacancy counterpart. But the V_X states do shift upward toward the CBM with decreasing inter-defect distance, $i.e.$, the distance of the V_X defect state to CBM is $V_X > SP > SD$. Thciteore, the closer the two vacancy sites are, the closer the V_X state is to the CBM.

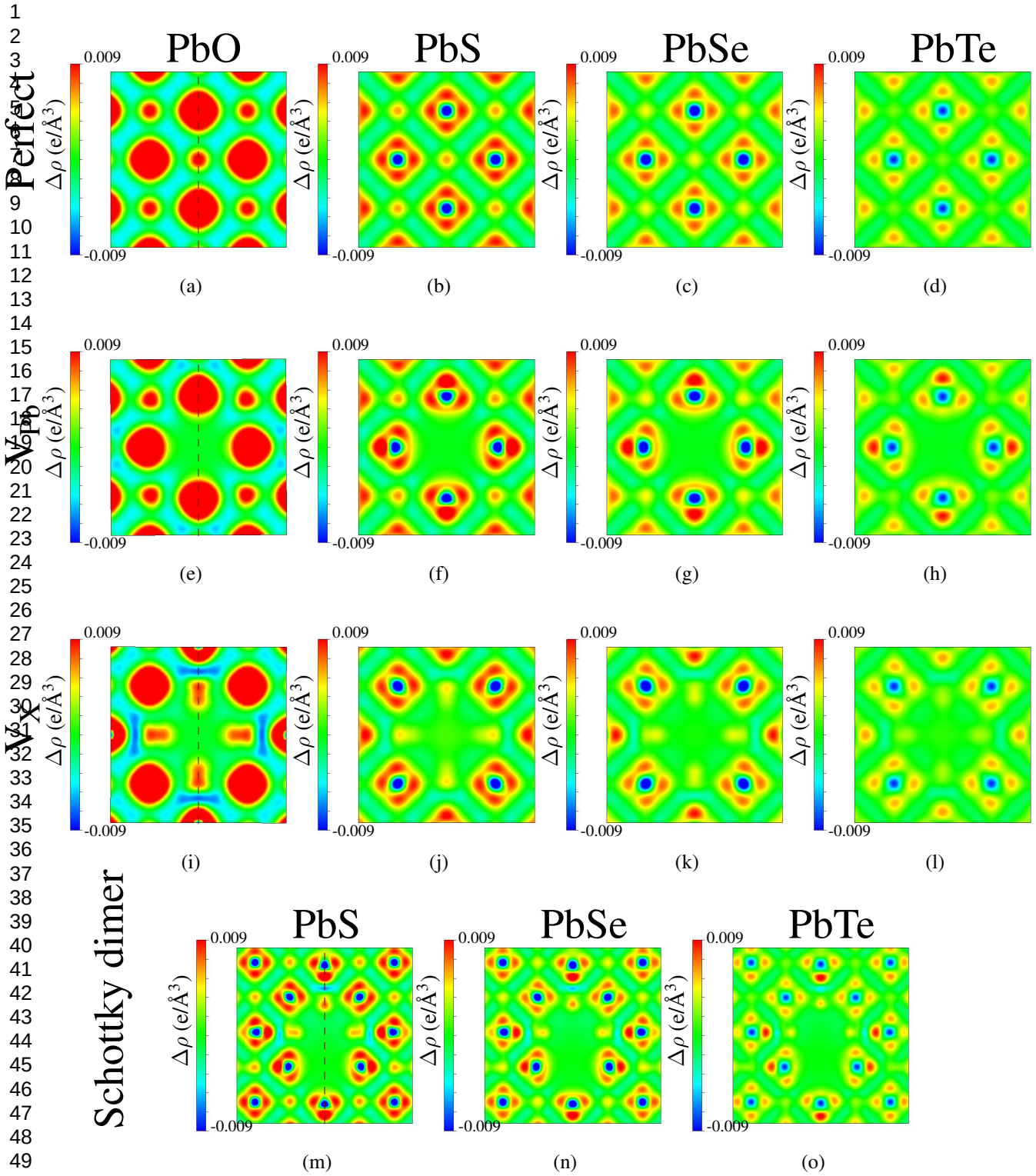

Figure 4. Charge density difference for perfect PbX systems, and PbX systems containing a V_{Pb}, V_X or a Schottky dimer. Color red denotes charge accumulation, and color blue for charge depletion. The cross-section is the (100) plane for perfect and V_{Pb}-containing systems, and is (001) for V_X containing systems. Dashed lines indicate the direction of the line profiles shown in Fig. 5

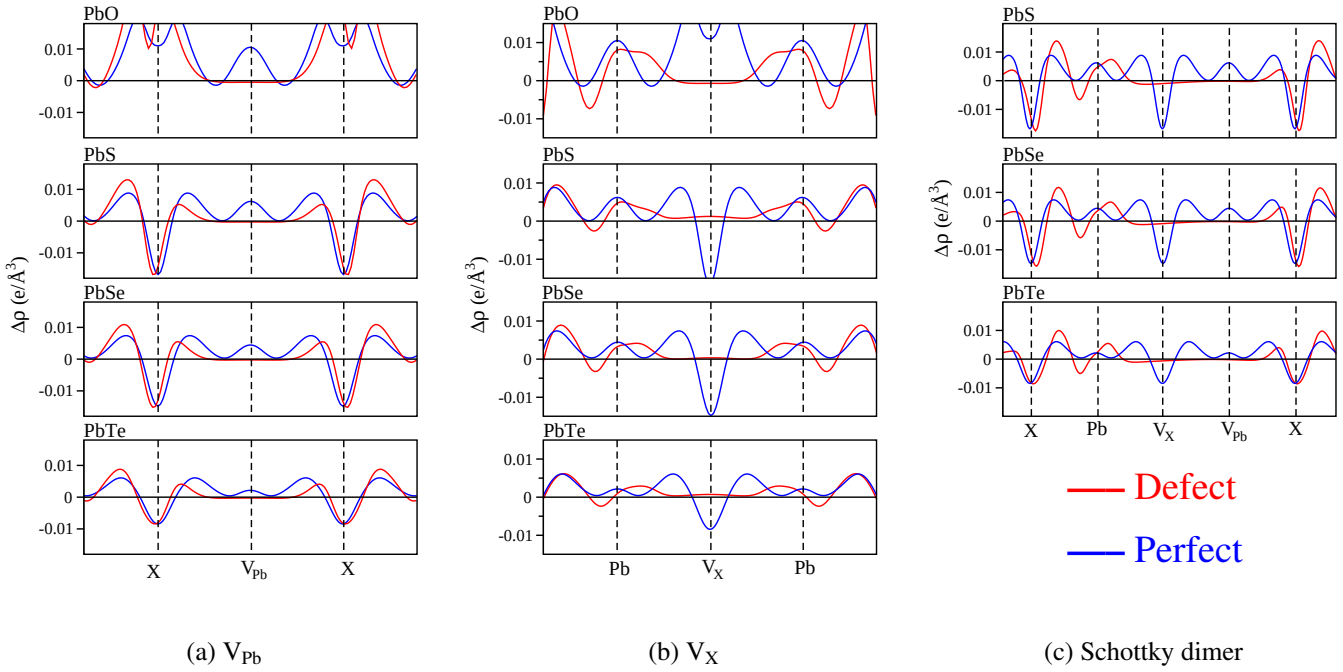

(a) V_{Pb} (b) V_X (c) Schottky dimer

Figure 5. Line profiles of $\Delta\rho$ for PbX systems containing a V_{Pb}, V_X or Schottky dimer. The lines are drawn along the dashed lines shown in Fig. 4 for different defect types.

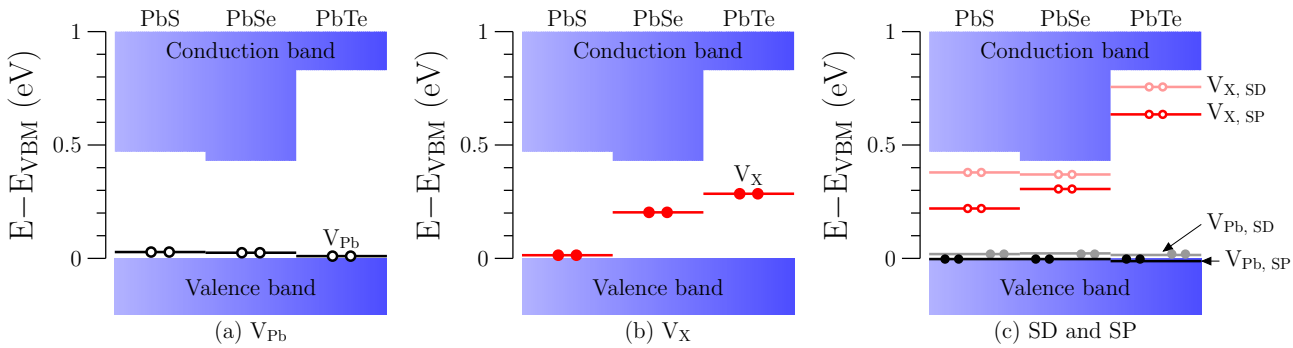

(a) V_{Pb} (b) V_X (c) SD and SP

Figure 6. Schematic of the defect states of (a) V_{Pb}, (b) V_X, and (c) Schottky dimer (SD) and Schottky pair (SP) in PbX systems at the L point of the first Brillouin zone. Energy of VBM is set at zero energy.

4. Discussions

4.1. Equilibrium defect concentration as a function of temperature

For the four kinds of stable defect chosen in this paper, we would give an estimate of their equilibrium concentration in bulk. The expression of free energy per atom f in terms of the equilibrium defect concentration x_d can be used for this purpose: (The readers are refered to the SI and Ref. [75] for a derivation.)

$$f = \frac{F}{n} = x_d E^f + k_B T[x_d \ln x_d + (1-x_d)\ln(1-x_d)], \quad (5)$$

where F is the total free energy of the system, n is the total number of atoms, k_B is the Boltzmann constant and T is the temperature in K. From the minimum of $f(x_d)$, we can determine the equilibrium defect concentration x_d at different

temperatures. Temperatures of 298 K, 500 K, 750 K and 1000 K were selected, and the results are shown both in Fig. 7 and Table 10. At first glance, the temperature dependence of x_d can be clearly seen, and the defect concentration increases with increasing temperature in an asymptotic manner. But overall speaking, the defect concentrations are very low: for PbS, for instance, the defect concentration at 500 K is 1.11×10^{-18} for V_{Pb}, 1.14×10^{-21} for V_S, 1.46×10^{-13} for Schottky dimer, and 1.43×10^{-18} for Schottky pair. These low concentrations imply that in nanocrystals which contain only tens of thousands of atoms, there will be not a single defect present in the PbX nanocrystals. The defect formation energy might be different on surfaces and in the bulk. As indicated by Hoang *et al.*, E^f for V_{Pb} at surface is 0.181 eV lower than that in the bulk, and the formation energy for V_{Te} is lowered by 0.207 eV. In future work, it would be useful to calculate defect formation energies also for surfaces and interfaces, to obtain a more complete understanding of defect energetices in PbX crystals. In addition, compound nanocrystals are in general not stoichiometric[11, 12], so that excess or depletion of one atomic species has to be accommodated either at the surface or in the interior of the nanocrystal.

The phase diagrams of PbX indicate that the stoichiometric configuration is very stable even at temperatures over 1000 K, implying that it is difficult for defects to be formed inside PbX lattices. This corresponds well to the low concentrations calculated here.

4.2. Coulomb model for Schottky defects

Since the inter-defect distance is a parameter that influences the physical propeties in stoichiometric defects, we attempt to explain its effect by a simple Coulomb model. The Schottky configurations are chosen for this purpose because they are more

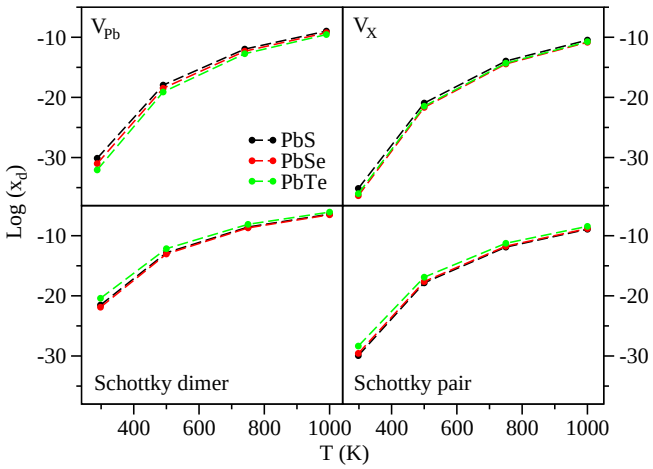

Figure 7. The equilibrium defect concentration x_d of the defective PbX systems at T =298 K, 500 K, 700 K and 1000 K. x_d is plotted on a logarithmic scale, and dashed lines are drawn to guide the eye.

stable than the Frenkel defect. We also took two more Schottky configurations named S2 and S3, with an inter-vacancy distance between Schottky dimer and Schottky pair, and the V_X site located on or near the body diagonal of the supercell, to obtain enough data points. The relationship between defect formation energy and inter-vacancy distance for the four Schottky defects are shown in Fig. 8. It is clear that E^f converges apace with increasing inter-vacancy distance, which indicates that the interaction between V_{Pb} and V_X is short-ranged. The formula used to calculate the Coulomb potential is

$$U = \frac{1}{4\pi\epsilon_0\epsilon} \sum_j \frac{q_v q_j^{NN}}{r}. \qquad (6)$$

This expression gives a Coulomb potential experienced by an vacancy site from its NNs , where $\frac{1}{4\pi\epsilon_0}$ is the Coulomb constant, ϵ is the dielectric constant of PbX systems (169, 204 and 414 at 300 K for PbS, PbSe, and PbTe, respectively[24]), q_v is the effective charge located on the V_X site, q_j^{NN} is the effective charge of the jth NN of the selected V_X, and r is the

Table 10. Equilibrium concentration of V_{Pb}, V_X, Schottky dimer and Schottky pair defects in PbX systems predicted by Eq. 5

PbX	V_{Pb}			V_X		
	298 K	500 K	1000 K	298 K	500 K	1000 K
PbS	7.47×10^{-31}	1.11×10^{-18}	1.05×10^{-9}	7.24×10^{-36}	1.14×10^{-21}	3.37×10^{-11}
PbSe	9.74×10^{-32}	3.29×10^{-19}	5.74×10^{-10}	4.47×10^{-37}	2.17×10^{-22}	1.47×10^{-11}
PbTe	8.74×10^{-33}	7.82×10^{-20}	2.80×10^{-10}	9.79×10^{-37}	3.45×10^{-22}	1.86×10^{-11}

PbX	Schottky dimer			Schottky pair		
	298 K	500 K	1000 K	298 K	500 K	1000 K
PbS	2.90×10^{-22}	1.46×10^{-13}	3.82×10^{-7}	1.14×10^{-30}	1.43×10^{-18}	1.20×10^{-9}
PbSe	1.30×10^{-22}	9.03×10^{-14}	3.00×10^{-7}	2.70×10^{-30}	2.38×10^{-18}	7.66×10^{-9}
PbTe	3.96×10^{-21}	6.92×10^{-13}	8.32×10^{-7}	4.49×10^{-29}	1.27×10^{-17}	3.57×10^{-9}

inter-defect distance in angstrom. The important parameter to be determined in Eq. 6 is the effective charges. The effective charge is defined as the charge difference on a certain atomic site before and after that atom is removed. For the effective charge located at the vacancy site, it is calculated by the following equation:

$$q_v = \Delta q_v - \sum_j \Delta q_j^{NN}, \qquad (7)$$

with $\Delta q_v = q_{atom} - q_{vac}$ the charge difference at the vacancy site, and Δq_j^{NN} the charge difference of the NNs of the vacancy. Thus, the formula takes into account both the contributions from the vacancy site itself and its NNs. q_{atom} is the Bader charge of the atoms in perfect PbX systems, and q_{vac} is integrated within a sphere at the vacancy site using the radii determined in Table 9. The results of q_v are listed in Table 11. But the Coulomb potential calculated using these effective charges are really low (ranging from 0.015 eV to 0.004 eV for different Schottky configurations and PbX systems) in comparison to the differences in E^f (in the range of 0.5 to 1.0 eV). Thciteore, variation in E^f as a function of separation cannot be explained by Coulomb models. Likely, lattice relaxation energies are dominating over electrostatic energies.

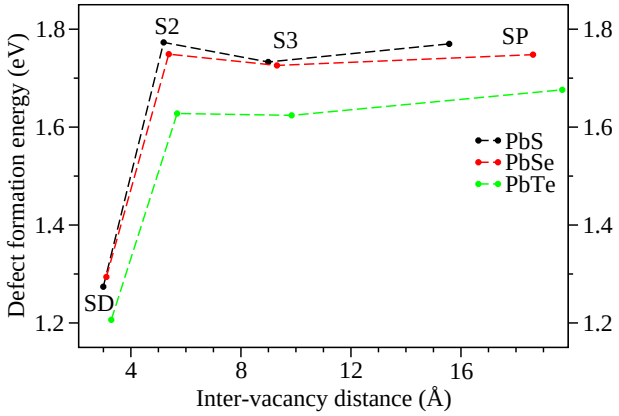

Figure 8. Defect formation energy versus inter-vacancy distance for the four different Schottky configurations. Dashed lines are drawn to guide the eye.

5. Conclusion

In this paper, we systematically studied the physical properties of a variety of defects in the PbX (X=S, Se, Te) systems by examining their defect formation energy, local geometry relaxation, charge transfer, and electronic structure. The studied defect types are vacancy, interstitial,

Table 11. Effective charge (q) of V_{Pb} and V_X in different Schottky configurations

PbX	Schottky dimer		Schottky.2		Schottky.3		Schottky pair	
	V_{Pb}	V_X	V_{Pb}	V_X	V_{Pb}	V_X	V_{Pb}	V_X
PbS	-0.74	0.71	-0.68	0.64	-0.74	0.84	-0.76	0.71
PbSe	-1.08	0.98	-1.60	1.32	-1.40	0.98	-1.46	0.95
PbTe	-0.82	0.60	-0.82	0.57	-0.85	0.67	-0.92	0.77

Schottky dimer and Schottky pair, and Frenkel defect. We draw the following conclusions that are of importance for the physical properties on PbX NCs.

(i) Photoluminescence

The relationship between the PL of PbX systems and their point defects is indicated in the SI and shown in Fig. 6 for the three most stable defects V_{Pb}, V_X and Schottky defects. The defect states of V_{Pb} are very shallow above the VBM with zero occupency, thus they are acceptor like and are likely to participate in a radiative recombination.[9] In contrast, the V_X defect states lie deeply in the band gap and are occupied by two electrons. Thciteore, these states are expected to trap the conducting holes in p-type PbX material, and thus reduce the PL quantum yield.[9] For the Schottky defects SP and SD, the constituent V_{Pb} and V_X form donor-acceptor pairs (DAP), wherein the electrons (holes) originally residing at the V_X (V_{Pb}) states are transffered to the V_{Pb} (V_X) states. These DAP's will act as the recombination center for the excited electrons and holes, and give rise to a PL emission with energy smaller than that of the material band gap[76]. It is noteworthy that the PL emission energy is related to the distance between V_{Pb} and V_X pair; larger inter-vacancy distance will result PL peaks with smaller energy. Although in the present study we only consider point defects in bulk, defects at surfaces, interfaces and defects therein may also play a role in the recombination process of PL in PbX[77, 78].

(ii) Off-stoichiometry

We have also investigated the energetics of off-stoichiometry for PbX bulk crystals. Table 3 indicates that the formation energy of V_{Pb} is smaller than V_X for all PbX systems, so an excess of anions is more easily accomodated than an excess of cations. Interstitials are unfavorable for both species. However, the defect energies are all quite high, so that off-stoichiometry is unfavorable. Phase separation may be hampered by nucleation barrier for the formation of pure Pb and X phases. For the case of NCs, part of the off-stoichiometry can be accomodated at the surface, also depending on the type of ligands used[11, 12]. The effects would be interesting to investigate in future studies.

(iii) Cation exchange

Considering all the defect formation energies, Schottky defects, SP and SD, are significantly lower in formation energy than the cation and anion vacancies. Thciteore, it becomes clear that Schottky defects may play a much more important role in the CE process than is currently presumed. This suprising result should be investigated into more detail in future studies, such as DFT simulations on migration energies, and MD simulations of CE.

(iv) Local geometry relaxation and charge deistribution at defects

Because of huge displacements of NN atoms around interstitial-type defects, anion and cation interstitial defects and Frenkel defects are less favored. The result of local relaxations showed that the expansion or contraction of the NNs of a defect site is a net result of the electrostatic in-

teraction among the atoms in that local environment. Bader charge analysis revealed that the degree of charge transfer decreases with O $\rightarrow$ S $\rightarrow$ Se $\rightarrow$ Te, in accordance with the trend of their electronegativity. Charge density difference plots indicated that charge density is locally polarized around the defect site, and electride type behavior with trapped charge is found at the anion vacancy site. In summary, we see a rich variety of physical properties introduced defects in the PbX semiconductor family, with direct implications for the synthesis and performance of PbX-containing HNCs.

In a future work, this study could be extended to charged defects, and to the calculation of energy barriers for migration of vacancy-type defects.

[1] Richard Dalven. *Solid State Physics*, volume 18. Academic, New York, 1973.

[2] Z.H. Dughaish. Lead telluride as a thermoelectric material for thermoelectric power generation. *Physica B*, 322:205, 2002.

[3] Tapas K. Chaudhuri. A solar thermophotovoltaic converter using pbs photovoltaic cells. *Int. J. Eng. Res.*, 16:481, 1992.

[4] H. Preier. Recent advances in lead-chalcogenide diode lasers. *Appl. Phys.*, 20:189, 1979.

[5] Shuchitangshu Chatterjee and Umapada Pal. Low-cost solar selective absorbers from indian galena. *Opt. Eng. (Bellingham)*, 32:2923, 1993.

[6] HyoJoong Lee, Henry C. Leventis, Soo-Jin Moon, Peter Chen, Seigo Ito, Saif A. Haque, Tomas Torres, Frank Nuesch, Thomas Geiger, Shaik M. Zakeeruddin, Michael Gratzel, and Md. Khaja Nazeeruddin. Pbs and cds quantum dot-sensitized solid-state solar cells: "old concepts, new results". *Adv. Funct. Mater.*, 19:2735, 2009.

[7] Marianna Casavola, Marijn A. van Huis, Sara Bals, Karel Lambert, Zeger Hens, and Daniël Vanmaekelbergh. Anisotropic cation exchange in pbse/cdse core/shell nanocrystals of different geometry. *Chem. Mater.*, 24:294–302, 2012.

[8] H. Groiss, E. Kaufmann, G. Springholz, T. Schwarzl, G. Hesser, F. Schäffler, W. Heiss, K. Koike, T. Itakura, M. Yano, and T. Wojtowicz. Size control and midinfrared emission of epitaxial pbte/cdte quantum dot precipitates grown by molecular beam epitaxy. *Appl. Phys. Lett.*, 91:222106, 2007.

[9] Timothy H. Gfroerer. *Photoluminescence in Analysis of Surfaces and Interfaces. In Encyclopedia of Analytical Chemistry*. John Wiley & Sons Ltd., Chichester, 2000.

[10] Celso de Mello Donegá. Synthesis and properties of colloidal heteronanocrystals. *Chem. Soc. Rev.*, 40:1512, 2011.

[11] Iwan Moreels, Karel Lambert, David De Muynck, Frank Vanhaecke, Dirk Poelman, José C. Martins, Guy Allan, and Zeger Hens. Composition and size-dependent extinction coefficient of colloidal pbse quantum dots. *Chem. Mater.*, 19:6101, 2007.

[12] Iwan Moreels, Bernd Fritzinger José C. Martins, and Zeger Hens. Surface chemistry of colloidal pbse nanocrystals. *J. Am. Chem. Soc.*, 130:15081, 2008.

[13] Dong Hee Son, Steven M. Hughes, Yadong Yin, and A. Paul Alivisatos. Cation exchange reactions in ionic nanocrystals. *Science*, 306:1009, 2004.

[14] Prashant K. Jain, Lilac Amirav, Shaul Aloni, and A. Paul Alivisatos. Nanoheterostructure cation exchange: Anionic framework conservation. *J. Am. Chem. Soc.*, 132:9997, 2010.

[15] Hongbo Li, Marco Zanella, Alessandro Genovese, Mauro Povia, Andrea Falqui, Cinzia Giannini, and Liberato Manna. Sequential cation exchange in nanocrystals: Preservation of crystal phase and formation of metastable phases. *Nano Lett.*, 11:4964, 2011.

[16] Karol Miszta, Dirk Dorfs, Alessandro Genovese, Mee Rahn Kim, and Liberato Manna. Cation exchange reactions in colloidal branched nanocrystals. *ACS NANO*, 5:7176, 2011.

[17] Sara Bals, Marianna Casavola, Marijn A. van Huis, Sandra Van Aert, K. Joost Batenburg, Gustaaf Van Tendeloo, and Daniël Vanmaekelbergh. Three-dimensional atomic imaging of colloidal coreshell nanocrystals. *Nano Lett.*, 11:3420, 2011.

[18] Esther Groeneveld, Leon Witteman, Merel Lefferts, Xiaoxing Ke, Sara Bals, Gustaaf Van Tendeloo, and Celso de Mello Donega. Tailoring znsecdse colloidal quantum dots via cation exchange: From core/shell to alloy nanocrystals. *ACS Nano*, 7:7913, 2013.

[19] Yingzhuo Sheng, Jumeng Wei, Bitao Liu, and Lingling Peng. A facile route to synthesize cdznse coreshell-like alloyed quantum dots via cation exchange reaction in aqueous system. *Mater. Rea. Bull.*, 57:67, 2014.

[20] Anil O. Yalcin, Zhaochuan Fan, Bart Goris, Wun-Fan Li, Rik S. Koster, Chang-Ming Fang, Alfons van

Blaaderen, Marianna Casavola, Frans D. Tichelaar, Sara Bals, Gustaaf Van Tendeloo, Thijs J. H. Vlugt, Daniël Vanmaekelbergh, Henny W. Zandbergen, and Marijn A. van Huis. Atomic resolution monitoring of cation exchange in cdse-pbse heteronanocrystals during epitaxial solid–solid–vapor growth. *Nano Lett.*, 14:3661, 2014.

[21] Florian D. Ott, Leo L. Spiegel, David J. Norris, and Setven C. Erwin. Microscopic theory of cation exchange in cdse nanocrystals. *Phys. Rev. Lett.*, 113:156803, 2014.

[22] E. Miller, K. Komarek, and I. Cadoff. Interrelation of electronic properties and defect equilibria in pbte. *J. Appl. Phys.*, 32:2457, 1961.

[23] A. Polity, R. Krause-Rehberg, V. Zlomanov, V. Stanov, and A. Chatchaturov. Study of vacancy defects in pbse and $pb_{1-x}sn_xse$ by positron annihilation. *J. Cryst. Growth*, 131:271, 1993.

[24] D. Khokhlov. *Lead Chalcogenides: Physics and Applications*. CRC Press, Washington, 2002.

[25] Seiji Yoneda, Masahiko Kato, and Isao J Ohsugi. Anomaly in the specific heat of lead tellurides. *J. Theo. Appl. Phys.*, 7:11, 2013.

[26] Bingpo Zhang, Chunfeng Cai, Shuqiang Jin, Zhenyu Ye, Huizhen Wu, and Zhen Qi. Resonant nature of intrinsic defect energy levels in pbte revealed by infrared photoreflectance spectroscopy. *Appl. Phys. Lett.*, 105:022109, 2014.

[27] D. Koumoulis, R. E. Taylor, Jr. D. King, and L.-S. Bouchard. Nmr study of native defects in pbse. *Phys. Rev. B*, 90:125201, 2014.

[28] Nelson J. Parada and Jr George W. Pratt. New model for vacancy states in pbte. *Phys. Rev. Lett.*, 22:180, 1969.

[29] Nelson J. Parada. Localized defects in pbte. *Phys. Rev. B*, 3:2042, 1971.

[30] Craig S. Lent, Marshall A. Bowen, Robert S. Allgaier, John D. Dow, Otto F. Sankey, and Eliza S. Ho. Impurity levels in pbte and $pb_{1-x}sn_xte$. *Solid State Commun.*, 61:83, 1987.

[31] Salameh Ahmad, S.D. Mahanti, Khang Hoang, and M.G. Kanatzidis. Ab initio studies of the electronic structure of defects in pbte. *Phys. Rev. B*, 74:155205, 2006.

[32] Zong-Ling Ding, Huai-Zhong Xing, Sheng-Lan Xu, Yan Huang, and Xiao-Shuang Chen. First-principles study of electronic properties in pbs($\bar{1}$00) with vacancy defect. *Chin. Phys. Lett.*, 24:3218, 2007.

[33] Khang Hoang, S.D. Mahanti, and Puru Jena. Theoretical study of deep-defect states in bulk pbte and in thin films. *Phys. Rev. B*, 76:115432, 2007.

[34] A. Walsh. Defect processes in a pbs metal organic framework: A quantum-confined hybrid semiconductor. *J. Phys. Chem. Lett.*, 1:1284, 2010.

[35] Haowei Peng, Jung-Hwan Song, M. G. Kanatzidis, and Arthur J. Freeman. Electronic structure and transport properties of doped pbse. *Phys. Rev. B*, 84:125207, 2011.

[36] J Berashevich, O Semeniuk, O Rubel, J A Rowlands, and A Reznik. Lead monoxide α-pbo: electronic properties and point defect formation. *J. Phys.: Condens. Matter*, 25:075803, 2013.

[37] E. O. Wrasse, R. J. Bairerle, A. Fazzio, and T. M. Schmidt. First-principles study of group iii impurity doped pbse: Bulk and nanowire. *Phys. Rev. B*, 87:085428, 2013.

[38] Donghun Kim, Dong-Ho Kim, Joo-Hyoung Lee, and Jeffrey C. Grossman. Impact of stoichiometry on the electronic structure of pbs quantum dots. *Phys. Rev. Lett.*, 110:196802, 2013.

[39] Su-Huai Wei and Alex Zunger. Electronic and structural anomalies in lead chalcogenides. *Phys. Rev. B*, 55:13605, 1997.

[40] E. A. Albanesi, C. M. I. Okoye, C. O. Rodriguez, and E. L. Peltzer y Blanca. Electronic structure, structural properties, and dielectric functions of iv-vi semiconductors: Pbse and pbte. *Phys. Rev. B*, 61:16589, 2000.

[41] Mohammed Lach-hab, Dimitrios A. Papaconstantopoulos, and Michael J. Mehl. Electronic structure calculations of lead chalcogenides pbs, pbse, pbte. *J. Phys. Chem. Solids*, 63:833, 2002.

[42] Kerstin Hummer, Andreas Grüneis, and Georg Kresse. Structural and electronic properties of lead chalcogenides from first principles. *Phys. Rev. B*, 75:195211, 2007.

[43] Yi Zhang, Xuezhi Ke, Changfeng Chen, and P. R. C. Kent J. Yang. Thermodynamic properties of pbte, pbse, and pbs: First-principles study. *Phys. Rev. B*, 80:024304, 2009.

[44] Jiaqing He, Li-Dong Zhao, Jin-Cheng Zheng, Jeff W. Doak, Haijun Wu, Hui-Qiong Wang, Yeseul Lee, Chris Wolverton, Mercouri G. Kanatzidis, and Vinayak P. Dravid. Role of sodium doping in lead chalcogenide thermoelectrics. *J. Am. Chem. Soc.*, 135:4624, 2013.

[45] Jonathan M. Skelton, Stephen C. Parker, Atsushi Togo, Isao Tanaka, and Aron Walsh. Thermal physics of the lead chalcogenides pbs, pbse, and pbte from first principles. *Phys. Rev. B*, 89:205203, 2014.

[46] Aron Walsh and Graeme W. Watson. Preparation of pbs-type pbo nanocrystals in a room-temperature ionic liquid. *J. Solid State Chem.*, 178:1422, 2005.

[47] G. Kresse and J. Hafner. *Ab initio* molecular-dynamics simulation of the liquid-metalamorphous-semiconductor transition in germanium. *Phys. Rev. B*, 49:14251, 1994.

[48] G. Kresse and J. Furthmüller. Efficiency of ab-initio total energy calculations for metals and semiconductors using a plane-wave basis set. *Comput. Mat. Sci.*, 6:15, 1996.

[49] G. Kresse and J. Furthmüller. Efficient iterative schemes for ab initio total-energy calculations using a plane-wave basis set. *Phys. Rev. B*, 54:11169, 1996.

[50] P.E. Blochl. Projector augmented-wave method. *Phys. Rev. B*, 50:17953, 1994.

[51] J.P. Perdew, K. Burke, and M. Ernzerhof. Generalized gradient approximation made simple. *Phys. Rev. Lett.*, 77:3865, 1996.

[52] A. Svane, N. E. Christensen, M. Cardona, A. N. Chantis, M. van Schilfgaarde, and T. Kotani. Quasiparticle self-consistent gw calculations for pbs, pbse, and pbte: Band structure and pressure coefficients. *Phys. Rev. B*, 81:245120, 2010.

[53] O. Madelung, U. Rössler, and M. Schulz. *Semiconductors: Group IV Elements, IV-IV and III-IV Compounds, Landolt-Börnstein, New Series, Group III, Vol. 41, Pt. A*. Springer-Verlag, Berlin, 2005.

[54] J. P. Perdew and A. Zunger. Self-interaction correction to density-functional approximations for many-electron systems. *Phys. Rev. B*, 23:5048, 1981.

[55] J. Heyd, G. E. Scuseria, and M. Ernzerhof. Hybrid functionals based on a screened coulomb potential. *J. Chem. Phys*, 118:8207, 2003.

[56] Jonathan M. Skelton, Stephen C. Parker, Atsushi Togo, Isao Tanaka, and Aron Walsh. Thermal physics of the lead chalcogenides pbs, pbse, and pbte from first principles. *Phys. Rev. B*, 89:205203, 2014.

[57] L. A. Constantin, J. M. Pitarke, J. F. Dobson, A. Garcia-Lekue, and J. P. Perdew. High-level correlated approach to the jellium surface energy, without uniform-gas input. *Phys. Rev. Lett.*, 100:036401, 2008.

[58] W. H. Strehlow and E. L. Cook. Compilation of energy band gaps in elemental and binary compound semiconductors and insulators. *J. Phys. Chem. Ref. Data*, 2:163, 1973.

[59] G. Kullerrud. The lead-sulfur system. *Am. J. Sci., Schairer Vol.*, 267-A:233, 1969.

[60] J.-C. Lin, R.C. Sharma, and Y.A. Chang. The pbs (lead-sulfur) system. *Bull. Alloy Phase Diagrams*, 7:374, 1986.

[61] J.-C. Lin, R.C. Sharma, and Y.A. Chang. The pb-se (lead-selenium) system. *J. Phase Equilib.*, 17:253, 1996.

[62] J.-C. Lin, K.-C. Hsieh, R.C. Sharma, and Y.A. Chang. The pb-te (lead-tellurium) system. *Bull. Alloy Phase Diagrams*, 10:340, 1989.

[63] Chris G. Van de Walle and Jörg Neugebauer. First-principles calculations for defects and impurities: Applications to iii-nitrides. *J. Appl. Phys.*, 95:3581, 2004.

[64] Fumiyasu Oba, Minseok Choi, Atsushi Togo, and Isao Tanaka. Point defects in zno: an approach from first principles. *Sci. Technol. Adv. Mater.*, 12:034302, 2011.

[65] C. M. Fang, M. A. van Huis, J. Jansen, and bergen H. W. Z. Role of carbon and nitrogen in fe_2c and fe_2n from first-principles calculations. *Phys. Rev. B*, 84:094102, 2011.

[66] Zhaochuan Fan, Anil O. Yalcin, Frans D. Tichelaar, Henny W. Zandbergen, Elise Talgorn, Arjan J. Houtepen, Thijs J. H. Vlugt, and Marijn A. van Huis. From sphere to multipod: Thermally induced transitions of cdse nanocrystals studied by molecular dynamics simulations. *J. Am. Chem. Soc.*, 135:5869, 2013.

[67] L. Chai, W. Al-Sawai, Y. Gao, A. J. Houtepen, P. E. Mijnarends, B. Barbiellini, H. Schut, L. C. van Schaarenburg, M. A. van Huis, L. Ravelli, W. Egger, S. Kaprzyk, A. Bansil, and S. W. H. Eijt. Surfaces of colloidal pbse nanocrystals probed by thin-film positron annihilation spectroscopy. *APL Materials*, 11:02211, 2013.

[68] Alex Kutana and Steven C. Erwin. Pbse nanocrystals remain intrinsic after surface adsorption of hydrazine. *Phys. Rev. B*, 83:235419, 2011.

[69] Naeemullah, G. Murtaza, R. Khenata, N. Hassan, S. Naeem, M.N. Khalid, and S. Bin Omran. Structural and optoelectronic properties of pbs_xse_{1-x}, pbs_xte_{1-x} and $pbse_xte_{1-x}$ via first-principles calculations. *Comp. Mater. Sci.*, 83:496, 2014.

[70] R.D. Shannon. Revised effective ionic radii and systematic studies of interatomic distances in halides and chalcogenides. *Acta Cryst.*, A32:751, 1976.

[71] Zhenyu Li, Jinlong Yang, J. G. Hou, and Qingshi Zhu. Inorganic electride: Theoretical study on structural and electronic properties. *J. Am. Chem.*

Soc., 125:6050, 2003.

[72] James L. Dye. Electrons as anions. *Science*, 301:607, 2003.

[73] Kimoon. Dicalcium nitride as a two-dimensional electride with an anionic electron layer. *Nature*, 494:336, 2013.

[74] Stephen G. Dale, Alberto Otero de-la Roza, and Erin R. Johnson. Density-functional description of electrides. *Phys. Chem. Chem. Phys.*, 16:14584, 2014.

[75] F. Smallenburg, L. Filion, M. Marechal, and M. Dijkstra. Vacancy-stabilized crystalline order in hard cubes. *P. Natl. Acad. Sci. USA*, 109:17886, 2012.

[76] Michael A. Reshchikov and Hadis Morkoç. Luminescence properties of defects in gan. *J. Appl. Phys.*, 97:061301, 2005.

[77] Michael M. Krause, Jonathan Mooney, and Patanjali Kambhampati. Chemical and thermodynamic control of the surface of semiconductor nanocrystals for designer white light emitters. *ACS Nano*, 7:5922, 2013.

[78] O. Voznyy, S. M. Thon, A. H. Ip, and E. H. Sargent. Dynamic trap formation and elimination in colloidal quantum dots. *J. Phys. Chem. Lett.*, 4:987, 2013.